Microchim Acta (2012) 177:211–219
DOI 10.1007/s00604-012-0774-9

ORIGINAL PAPER

A nanoporous ruthenium oxide framework for amperometric sensing of glucose and potentiometric sensing of pH

Jun Ho Shim · Minkyung Kang · Youngmi Lee · Chongmok Lee

Received: 15 September 2011 / Accepted: 28 January 2012 / Published online: 15 February 2012

Abstract Nanoporous ruthenium oxide frameworks (L_2-eRuO) were electrodeposited on gold substrates by repetitive potential cycling in solutions of ruthenium(III) ions in the presence of reverse neutral micelles. The L_2-eRuO was characterized in terms of direct oxidation of glucose and potentiometric response to pH values. The surface structures and morphologies of the L_2-eRuO were characterized by scanning electron microscopy, energy dispersive X-ray spectroscopy, Raman spectroscopy, and high-resolution transmission electron microscopy. Their surface area was estimated via underpotential deposition of copper. L_2-eRuO-modified electrodes showed a 17-fold higher sensitivity (40 μA mM^{-1} cm^{-2} towards glucose in 0–4 mM concentration in solution of pH 7.4) than a RuO electrode prepared in the absence of reverse micelles. Potential interferents such as ascorbic acid, 4-acetamidophenol, uric acid and dopamine displayed no effect. The new electrode also revealed improved potentiometric response to pH changes compared to a platinum electrode of the same type.

J. H. Shim and M. Kang are equally contributed to this work.

Electronic supplementary material The online version of this article (doi:10.1007/s00604-012-0774-9) contains supplementary material, which is available to authorized users.

J. H. Shim · M. Kang · Y. Lee (✉) · C. Lee (✉)
Department of Chemistry and Nano Science,
Ewha Womans University,
Seoul 120-750, Korea
e-mail: youngmilee@ewha.ac.kr
e-mail: cmlee@ewha.ac.kr

J. H. Shim
Department of Chemistry,
Daegu University,
Gyeongsan 712-714, Korea

Keywords Nonenzymatic amperometric glucose sensor · Nanoporous ruthenium structures · Copper underpotential deposition · Potentiometric pH sensing

Introduction

Enzyme electrodes using glucose oxidase (GOx), alcohol dehydrogenase and other enzymes have been of analytical significance and widely employed for the electrochemical sensors, however, have crucial disadvantage of instability owing to the nature of enzyme. GOx based electrochemical sensors have additional drawback of oxygen dependence or necessity of mediator [1]. Thus, it would be desirable to determine bio-molecule concentration without using enzymes. For some recent examples of the electrochemical glucose sensors, GOx-free sensors have been developed using meso/nanoporous Pt films deposited in the presence of suitable surfactants [2–5], three-dimensional (3D)-network electrodes with various bimetallic compositions [6], highly dispersed metallic nanoparticles on composite film of carbon nanotubes (CNTs) [7, 8], nanoporous gold film electrode [9–11], metal-functionalized graphene nanohybrids [12], and metal nanoparticles incorporated into the porous carbon support [13, 14]. Among them, highly porous metallic nanocomposites are of great interest due to the selective/sensitive enhancement of kinetically sluggish heterogeneous faradic reactions including electrochemical glucose oxidation [2–6, 15, 16].

In particular, porous nanostructured materials based on Pt by electrochemical deposition have been intensively investigated with the aid of surfactant as a suitable template, such as hexagonal (H_1) lyotropic liquid crystalline (LLC) phase [17, 18], potential-controlled surfactant assembly [19], and reverse micelle (L_2) solution of a nonionic surfactant [4, 5, 19]. Pt thin films with hexagonally ordered nanopores (one-dimensional,

1D) on the scale of a few nanometers from both LLC template and the micelle-type aggregation were produced, so-called H_1-ePt [3]. Highly desirable 3D-nanoporous Pt films, namely L_2-ePt [4], were formed by simply electroplating in a L_2 phase solution, where detailed studies regarding morphologies and roughness factors were also investigated [5, 20]. It is notable, however, there have been no reports regarding 3D-nanoporous metal films electroplated from L_2 solution except Pt.

Ruthenium oxide has received attention for catalytic applications [21, 22] and pH measurements [23] due to its metallic conductivity and thermal stability. As far as we know, no porous RuO_2 electrode has been reported except macroporous Ru oxide electrode for pH and NADH sensing via templates by the controlled evaporation (CE) and Langmuir-Blodgett (LB) technique [24]. In this study, we have applied simple fabrication method for 3D-nanoporous Ru oxide film, L_2-eRuO, using a reverse micelle surfactant procedure, where several day evaporation time in CE technique or the LB trough in LB technique are not necessary. The pore diameter and widths of interstitial nanoparticles on an L_2-eRuO film have been analyzed through a high-resolution transmission electron microscopy (HR-TEM) and the surface area of the electrodes was estimated by Cu underpotential deposition (UPD) [25, 26]. The electroplated L_2-eRuO film possesses considerably high real surface area, and it could enhance the kinetically controlled electro-oxidation of glucose, which is demonstrated in this presentation together with pH sensing.

Experimental

Reagents

Ruthenium chloride hydrate ($RuCl_3\ xH_2O$), Trition X-100, sodium dihydrogen phosphate ($NaH_2PO_4\ H_2O$), sodium hydrogen phosphate (Na_2HPO_4), citric acid, boric acid, D-(+)-glucose, L-ascorbic acid (AA), 4-acetamidophenol (AP), uric acid (UA), and dopamine hydrochloride (DA) were purchased from Sigma-Aldrich (St. Louis, MO, USA http://www.sigma-aldrich.com). $CuSO_4$ (anhydrous) was supplied by Junsei Chemical Co., Ltd (http://junsei.lookchem.com). All other chemicals used were of analytical grade, all solutions were prepared with deionized water (resistivity ≥18 MΩ cm).

Electrochemical deposition of ruthenium and electrochemical measurements

Thin films of L_2-eRuO were formed by electroplating in a similar method described previously for L_2-ePt [4]. Briefly, in a solution containing a ruthenium precursor ($RuCl_3$), Triton X-100, and NaCl aqueous solution (5:45:50 in wt%, at 40 °C), the nanoporous metal oxide was deposited on a Au disk electrode (1.6 mm in diameter, Bioanalytical Systems, Inc. http://www.basinc.com) by scanning the potentials from +0.0 to −0.8 V at a scan rate of 50 mV s^{-1}. The numbers of potential cycling were varied from 5 to 70, in order to obtain the L_2-eRuO films with different roughness factor (*Rf*). The Triton X-100 used was extracted by placing the electrode deposited with nanoporous metals in distilled water, which was replaced with fresh water every 2 h for 4–5 times. Then, the electrodes were electrochemically cleaned in 0.1 M H_2SO_4 by scanning the potentials from +0.0 to +1.5 V at a scan rate of 50 mV s^{-1} to remove the remained surfactant before performing other experiments. A saturated calomel reference electrode (SCE) and Pt wire counter electrode were used. UPD of Cu on as-prepared L_2-eRuO electrode was performed in 2 mM $CuSO_4$/0.1 M H_2SO_4. The amperometric response of the prepared electrode to varying glucose concentration was measured at +0.5 V (vs. SCE) with the successive addition of a glucose standard solution into a 0.05 M phosphate buffer solution (pH 7.4) with constant stirring. The electrode pH response was obtained by titrating a universal buffer composed of 11.4 mM boric acid, 6.7 mM citric acid, 10.0 mM NaH_2PO_4 with small aliquots of NaOH and HCl while monitoring the electrode potentials (vs. Ag/AgCl reference electrode). Thin films of L_2-eRuO were also formed on a Au wire (0.5 mm in diameter, Aldrich) to check pH response. The solutions were stirred magnetically and the equilibrium potentials were recorded.

Characterization

The electroplated L_2-eRuO film structures were examined by field emission scanning electron microscopy (FE-SEM, Jeol JSM-6700F http://www.jeol.com), which was equipped with an energy dispersive X-ray spectroscopy (EDS) system, and HR-TEM (Jeol JEM-2100F, 200 kV). FT Raman spectroscopy (Renishaw InVia Sustem http://www.renishaw.com) was used to characterize the RuO materials. The electrochemical measurements were performed using a CHI 705 workstation (CH Instruments http://www.chinstruments.com). All experiments were carried out in a Faraday cage to increase the signal-to-noise (*S/N*) ratio. For the potentiometric measurements, the potential differences between the working electrode and Ag/AgCl reference electrode were measured using a PC equipped with a high-impedance input 16-channel analog-to-digital converter (KOSENTECH Inc., Korea http://www.physiolab.co.kr).

Results and discussion

FE-SEM images of the surface morphology of the RuO films grown on polished gold substrate obtained in 0.2 wt % and 5 wt% $RuCl_3$ by repetitive potential cycling in the absence of the surfactant are depicted in Fig. 1a and b,

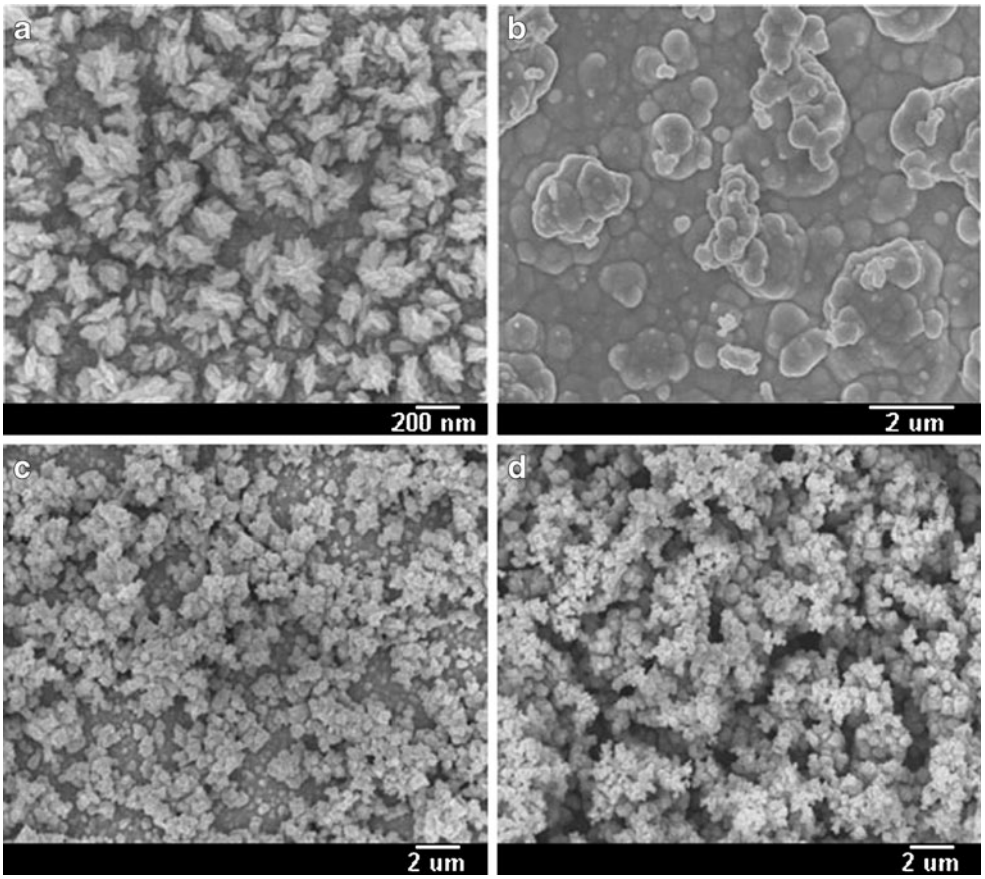

Fig. 1 FE-SEM images of the electroplated Ru oxide film electrodes induced in the absence (**a** and **b**) and presence (**c** and **d**, 50 wt%) of surfactant: RuO images electroplated in an aqueous solution containing low (**a**, 0.2 wt%) and high concentration (**b**, 5 wt%) of $RuCl_3$; L_2-eRuO images (obtained in an aqueous solution containing 5 wt% $RuCl_3$ and 50 wt% surfactant) taken before (**c**) and after (**d**) electrochemical cleaning by voltammetric cycling in 0.1 M H_2SO_4

respectively. It is observed that typical surface morphology of Ru film obtained from low concentration of $RuCl_3$ (Fig. 1a) is obviously different from that from high concentration (Fig. 1b). Although Ru film in Fig. 1a was found to have relatively a little rough surface and a lot of protruding spikes compared to that obtained from higher concentration of Ru precursor as shown in Fig. 1b, no obvious porous structure was found even at high concentration of $RuCl_3$. These deposits result from uninhibited and more vigorous metal growth over the electrode substrates in the absence of surfactants which direct the metal structure and increase electroplating solution viscosity.

Electroplating of Ru with the aid of a surfactant template onto polished gold electrodes was also conducted by potential sweep method rather than constant potential method, which was used widely in previous reports, owing to the improved stability of the films [27]. The ternary plating systems used in our experiments were consisted of a 5 wt% $RuCl_3$, 50 wt% Triton X-100, and 45 wt% NaCl. After electroplating, the electrodes were rinsed to remove the remained surfactant with copious amounts of deionized water followed by further cleaned using a cycling potential between +0.0 V and +1.5 V (vs. SCE) in 0.1 M H_2SO_4 until reproducible cyclic voltammograms were obtained. The surface morphologies for the L_2-eRuO were observed using FE-SEM before and after the electrochemical cleaning process as shown in Fig. 1c and d, respectively. EDS confirmed that no surfactant was present in the washed films (Fig. 1d). The electrochemical cleaning resulted in a deeper porosity with uniform nanoparticle distribution within L_2-eRuO film. Indeed, the L_2-eRuO film was composed of Ru nanoparticles interconnected with each other. Note that these FE-SEM images of L_2-eRuO are contrast to that of L_2-ePt [4] where no apparent grain or pore was observed.

TEM studies (Fig. 2a–c) supported that the electroplated L_2-eRuO film revealed a highly porous structure consisting of regular holes of 2.0 (±0.2) nm in diameter. The interstitial nanopores among the partially merged Ru nanoparticles are quite evenly distributed, and their width is about 2.3 (±0.2) nm. The resulting morphology is supposed to be related to their catalytic activities of nanostructured Ru toward direct glucose oxidation. More detailed discussion regarding electrocatalytic glucose sensor is described in a later section. In addition, Raman spectra in Fig. 2d clearly shows the three major Raman peaks corresponding to crystalline Ru oxide in the rutile form (E_g, A_{1g}, and B_{2g}, modes are located at 508, 622 and 687 cm^{-1}, respectively). HR-TEM results in Fig. 2c agree with the crystalline structures of the L_2-eRuO film.

The Cu UPD on the L_2-eRuO film for determining the real surface area (RSA) is a relatively effective technique over other methods such as CO stripping, hydrogen adsorption and Brunauer-Emmett-Teller (BET), owing to the similarity of the atomic radii (Cu, 128 pm; and Ru, 134 pm) [26]. Fig. 3a

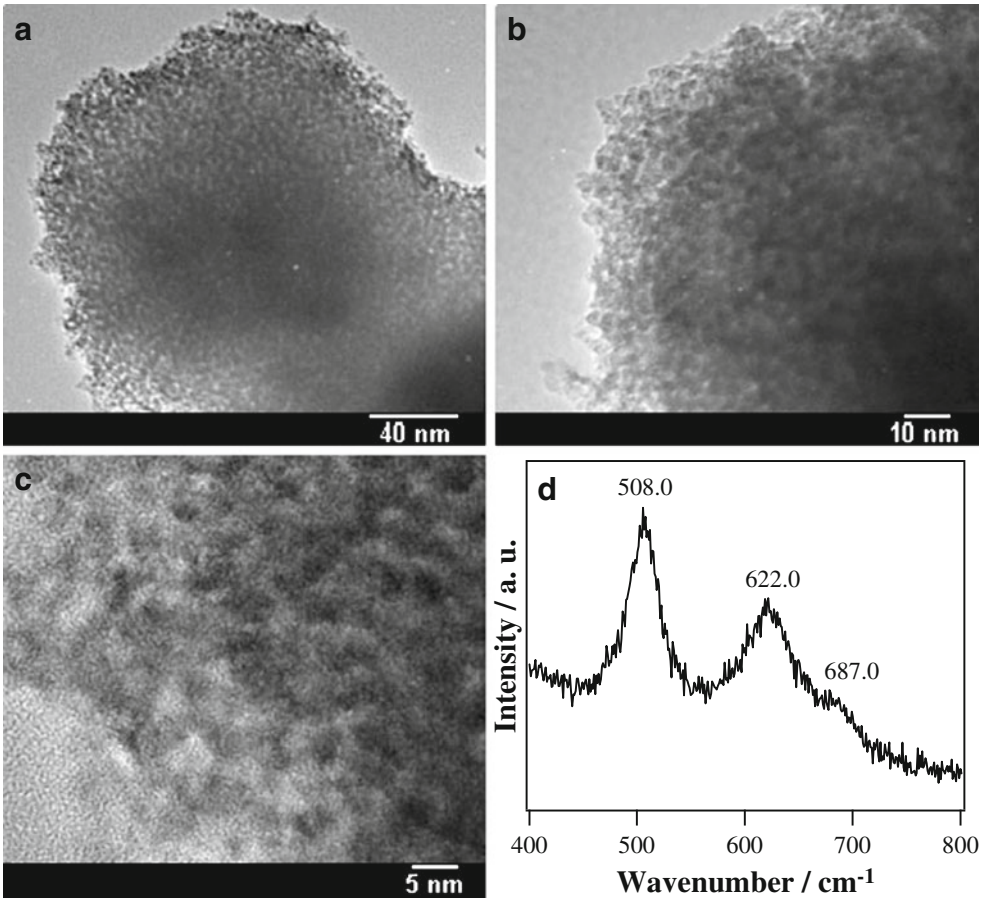

Fig. 2 TEM images (**a**–**c**) corresponding to the L_2-eRuO showing the detailed actual nanoporous morphology at three-different magnifications. Raman spectrum (**d**) showing the three major Raman peaks corresponding to crystalline Ru oxide

presents that the Cu surface coverage is determined using cyclic voltammetry (CV) in 0.1 M H_2SO_4/2 mM $CuSO_4$ solution purged by N_2 at a potential scan rate of 10 mV s^{-1} on the L_2-eRuO electrode to find out what the potential range of Cu UPD growth is. The CV scans began at 0.4 V vs. SCE, moved gradually in cathodic direction and then reversed to anodic direction at various switching potentials to allow repetitive deposition/desorption of Cu^{2+} ions to take place on the L_2-eRuO electrode surface. Presented L_2-eRuO film (as shown in Fig. 1d) was prepared from surfactant-assisted $RuCl_3$ solution by scanning the potentials from +0.0 V to −0.8 V for 30 cycles at a scan rate of 50 mV s^{-1}. It is accepted that UPD of metals starts in a potential region more positive than the Nernst potential by forming a monolayer. Indeed, the calculated equilibrium Nernst potential for Cu^{2+}/Cu is around 0.016 V (vs. SCE) for 2 mM $CuSO_4$ solution, and the first cathodic current increase from +0.2 V (vs. SCE) is assigned as a Cu UPD on the L_2-eRuO surface. The deposited Cu atoms were stripped from Ru surface at around +0.15 V (vs. SCE) when the electrode was subjected to the reverse anodic scan. A strong oxidation peak of the deposited Cu overlayers on the anodic scan was not observed readily on 3D-nanoporous Ru electrode surface probably owing to the relatively large density of the oxide overlayers with high surface area to volume ratios, as discussed in previous study [27]. In this experiment, a large charging capacitance current background was observed, indicating that the conductive Ru oxide with large surface area was formed during the electroplating process. The Cu surface coverage on L_2-eRuO film surface as displayed in Fig. 3b was calculated from the integrated charge of UPD stripping peak after subtracting its background. The surface coverage of Cu UPD increases with more negative switching potential and reaches a plateau of ca. 1.1×10^{-8} mol·cm^{-2} or 2.1 mC·cm^{-2} beyond −0.05 V (vs. SCE). This surface coverage can be calculated as 0.91 monolayer of Cu using the conversion factor in the literature [25].

As-prepared L_2-eRuO electrode was tested for a non-enzymatic amperometric glucose sensor. To determine the appropriate glucose oxidation potential, the amperometric response depending on the applied potentials (varied from +0.3 to +0.7 V with a step of 0.1 V) was measured at an L_2-eRuO electrode prepared by 30 CV cycles in 0.05 M phosphate buffer solution (pH 7.4) containing 2.0 mM glucose. The glucose oxidation current gradually increases at more positive potential (data not shown). For example, the amperometric response at +0.6 V or +0.7 V showed three fold higher than that at +0.5 V, however, stability of current response and *S/N* ratio at +0.5 V seems to be better than that at +0.6 or +0.7 V. Furthermore, it is well-known that the susceptibility to interference species decreases with lowering detection potential of

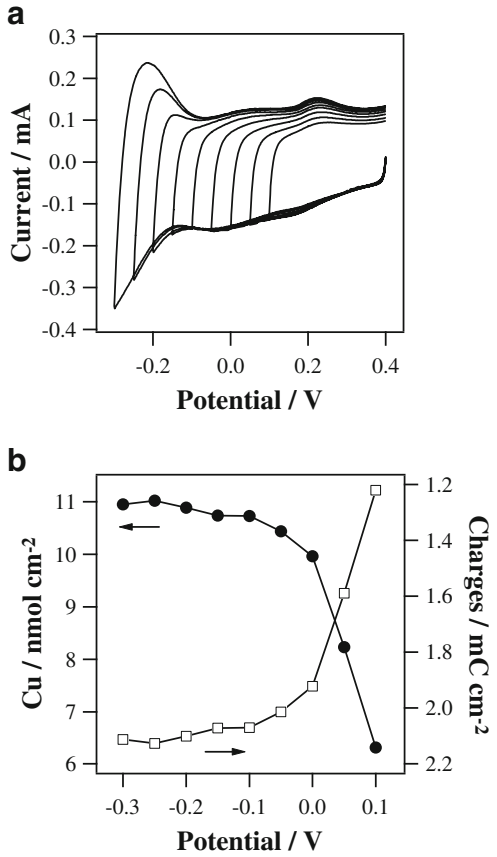

Fig. 3 Cyclic voltammograms (**a**) and Cu surface coverage vs. cathodic switching potentials (**b**) obtained from L_2-eRuO electrode immersed in a 2 mM $CuSO_4$/0.1 M H_2SO_4 solution at a scan rate of 10 mV s^{-1}. The Cu surface coverage on nanoporous Ru surface was calculated from the integrated charge of UPD stripping peak (ca. 0.220 V vs. SCE) after subtracting its background

the sensor. Hence the applied potential for glucose sensing was fixed at +0.5 V for all subsequent experiments.

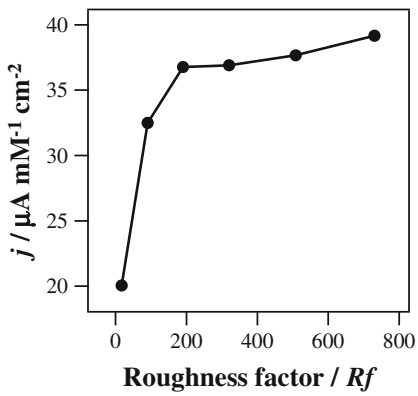

Fig. 4 Dependence of glucose sensitivities (normalized to GSA) on *Rf* values of L_2-eRuO, which were varied by changing the number of CV cycles (5, 10, 20, 30, 50, and 70 from the left to the right, respectively) for electroplating. Glucose sensitivity of L_2-eRuO was examined by successive adding 0.25 mM glucose in 0.05 M phosphate buffer solution (pH=7.4) at +0.5 V (vs. SCE)

The sensor sensitivity (from 0 to 4 mM) depending on the number of the repetitive CV cycles during the preparation process was also examined to find optimum preparation condition (Fig. 4). For this, the L_2-eRuO films were prepared on Au disk electrodes by 5, 10, 20, 30, 50, and 70 CV cycles, respectively, and the geometric surface area (GSA) of each electrode was determined by chronocoulometric analysis as described previously [28]. As aforementioned, the RSA of each electrode was estimated using the Cu UPD on L_2-eRuO. The *Rf* value of each electrode was calculated by dividing RSA by GSA. The (number of CV cycles, *Rf*) data are (5, 17.4), (10, 90.4), (20, 191), (30, 320), (50, 508), and (70, 731), respectively. Interestingly, *Rf* value was roughly hundred times of the number of CV cycles except for the initial stage of film growth. The sensor sensitivity (current response vs. glucose concentration) was normalized to the corresponding RSA (*j*). As seen in Fig. 4, the sensitivity increases with a *Rf* increase, and the sensitivity enhancement was large at *Rf*< 200, while increment of the sensor sensitivity became much smaller at *Rf* >200. For all subsequent experiments, thus the

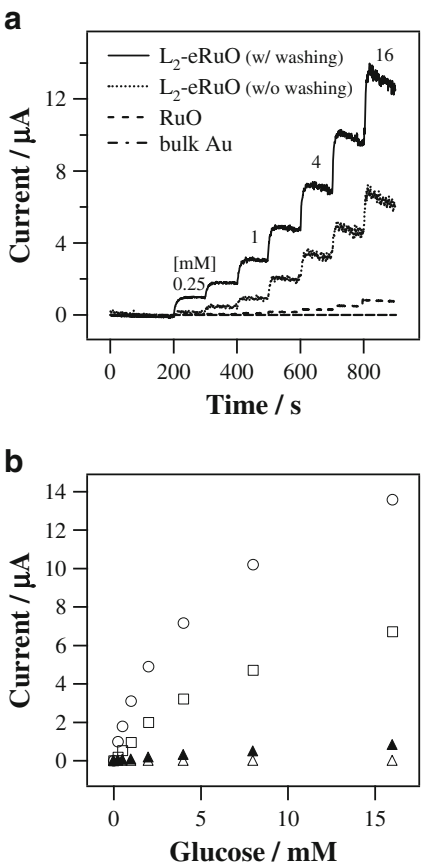

Fig. 5 Amperomeric current responses (**a**) and calibration curves in terms of glucose concentration (**b**) at the bulk Au, RuO, L_2-eRuO (without electrochemical cleaning) and L_2-eRuO (with electrochemical cleaning) in deoxygenated 0.05 M phosphate buffer solution (pH=7.4) at +0.5 V (vs. SCE)

number of repetitive CV cycles in L_2-eRuO electrode was fixed at 30 (Rf = 320).

Figure 5a presents typical dynamic steady-state current response curves (i-t curves) of four types of electrodes to consecutive increments in glucose concentration. Four electrodes used are bulk Au, RuO without surfactant, L_2-eRuO (not electrochemically cleaned), and L_2-eRuO (electrochemically cleaned in H_2SO_4) for comparison. The applied potential was +0.5 V to minimize interferent oxidation and the measurements were carried out in a deoxygenated 0.05 M phosphate buffer solution. The glucose concentrations were changed from zero to 16 mM by the successive additions of a pre-calculated amount of the glucose stock solution, considering that the normal physiological level of glucose is 3–8 mM [3]. Figure 5b shows the corresponding calibration plots for the amperometric detection of glucose at those four electrodes. The overall current responses in the range of zero to 16 mM glucose were 0.8 and 13.5 μA at RuO without surfactant and L_2-eRuO (electrochemically cleaned in H_2SO_4) electrode, respectively. The electrochemically cleaned L_2-eRuO electrode showed 16.9 fold higher electrocatalytic activities than RuO without surfactant. The sensitivity of 40.2 μA mM^{-1} cm^{-2} (normalized to GSA) was obtained at the electrochemically cleaned L_2-eRuO electrode in a linear range of zero to 4 mM glucose with a detection limit of approximately 21 μM glucose (*S/N*=3). This sensitivity value is comparable with those of the reported nanostructured gold electrodes [29]. For example, comparison of analytical performance of our sensor with other published nonenzymatic glucose sensors is summarized in Table 1. The developed method in this work exhibits the characteristics of the good sensitivity and interference resistance under biological conditions, especially at physiological pH.

The other positive characteristics of L_2-eRuO electrode is the selectivity against biological interferents. The anionic (AA and UA), neutral (AP) and cationic (DA) molecules in biological samples could be oxidized easily at relatively positive potentials and often interfere with glucose detection: for our glucose sensors, +0.5 V vs. SCE. Figure 6 shows the effects of the interfering species, where the injection of interferents was performed while monitoring the amperometric response in phosphate buffer solution containing 5 mM glucose. The injection of AA (100 μM), AP (100 μM), UA (20 μM), and DA (20 μM) did not cause serious change in the current response. Note that the normal physiological levels of the above four interferents are commonly below the injected amounts. In addition, to exclude the possibility of saturation after the last addition of glucose, we compared the amperometric responses between glucose only and the mixture of analyte and four interfering substances because the real sample contains both analyte and interfering species. As shown in Fig. 7, the amperometric responses between these two samples were virtually the

Table 1 Comparison of the reported nonenzymatic glucose sensors recently

Electrode assembly[a]	Sensitivity[b]	Linear range	LODs (μM)	Interferences[d]	Applied potential	Supporting electrolyte	Ref
GCE/Cu-CuO NWs/Nafion	8.59 μA mM^{-1}	0.1 mM–12 mM	50	<5%	0.30 V (vs SCE)	0.1 M NaOH	[30]
GCE/Au@Pd-ILs-Au@Pd	nr[c]	5 nM–50 μM	1000	>5%	0.0 V (vs Ag/AgCl)	0.1 M phosphate[e]	[31]
CuO/Cu	761.9 μA mM^{-1} cm^{-2}	2 μM–20 mM	1	<5%	0.70 V (vs Ag/AgCl	0.1 M NaOH	[32]
SPE/tubular Pd	nr	0.1 mM–58 mM	80	<5%	0.60 V (vs SCE)	0.1 M phosphate	[33]
Porous AuNPs-CS/Pt HNPCs/Nafion	nr	3.0 μM–7.7 mM	1	<5%	0.35 V (vs SCE)	0.1 M phosphate	[34]
GCE/Gr/Ni(II)-Qu	187 nA $μM^{-1}$	3 μM–900 μM	0.5	nr	nr (vs SCE)	0.1 M NaOH	[35]
GCE/Nafion/MCV/PtPd	0.11 μA mM^{-1} cm^{-2}	1.5 mM–12 mM	120	< 5%	0.55 V (vs Ag/AgCl)	0.1 M phosphate	[36]
GCE/npAu-Ru	240 μA mM^{-1} cm^{-2}	0 mM–6 mM	1.7	<5%	−0.10 V (vs SCE)	0.05 M phosphate	[11]
Au/npRu	40.2 μA mM^{-1} cm^{-2}	0 mM–4 mM	21	<5%	0.50 V (vs SCE)	0.05 M phosphate	f

[a] GCE, glassy carbon electrode; ILs, ionic liquids; SPE, screen printing electrode; CS, chitosan; HNPCs, hollow nanoparticle chains; Gr, graphene; Qu, Quercetin; MCV, mesoporous carbon vesicle

[b] Sensor's sensitivity depends on the surface area

[c] Not reported

[d] Estimated from the data presented, *i.e.* below 5% when 2–5 mM glucose and 100 μM AA were used

[e] Phosphate buffer solution

[f] This work.

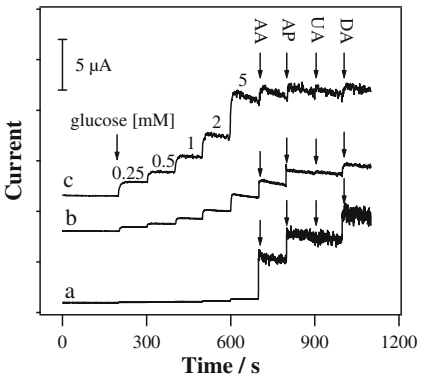

Fig. 6 Amperometric current responses with the injection of glucose and interfering species at the (**a**) RuO, (**b**) L_2-eRuO (without electrochemical cleaning) and (**c**) L_2-eRuO (with electrochemical cleaning) in deoxygenated 0.05 M phosphate buffer solution (pH=7.4) at+0.5 V (vs. SCE). Added concentration is AA (100 μM), AP (100 μM), UA (20 μM), and DA (20 μM)

same each other. We also have measured the amperometric responses between the analyte and the mixture of analyte and a specific interfering substance, *i.e.*, AA, AP, AU, or DA, where the differences were hard to be observed (Fig. S1 in Electronic Supplementary Material, ESM).

Such selectivity of sensing against interferents stems from the nature of electron-transfer [3]. Briefly, glucose oxidation without enzyme is a sluggish electron-transfer reaction, *i.e.*, kinetic-controlled electrochemical system, which is different from the electrode reaction of other interfering species, *i.e.*, diffusion-controlled electrochemical system. Therefore, the electrode with nanoporous structure could selectively enhance the faradaic current of non-enzymatic glucose oxidation since the interfering species should be depleted inside the diffusion layer.

The potentiometric responses of the L_2-eRuO electrode to pH were examined from pH 2 to 11 by adding aliquots of

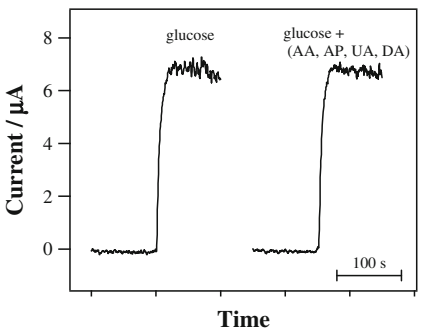

Fig. 7 Comparison of amperometric current responses between the injection of glucose (5 mM) only (*left*) and a mixture of glucose (5 mM) + four interference species (*right*) at the L_2-eRuO (with electrochemical cleaning) in deoxygenated 0.05 M phosphate buffer solution (pH=7.4) at +0.5 V (vs. SCE) with interfering species mixture of AA (100 μM), AP (100 μM), UA (20 μM), and DA (20 μM)

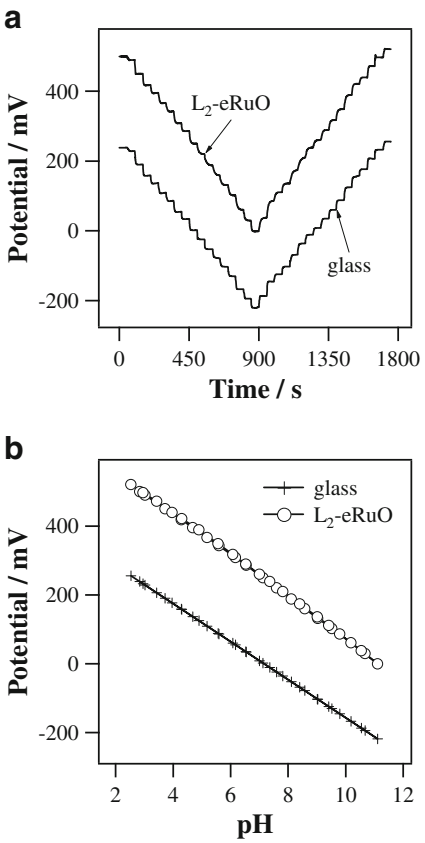

Fig. 8 Comparison of the pH responses between a glass pH electrode and an L_2-eRuO: dynamic potentiometric responses towards varying pH values (**a**); and calibration curves (**b**) corresponding to (**a**). The pH changes were realized by additions of NaOH and HCl solution to a universal buffer solution

NaOH to a universal buffer solution. Again, pH was changed reversely from 11 to 2 by adding HCl to check the reliability, where no hysteresis of pH response was observed. Figure 8 shows the typical potentiometric response curves for L_2-eRuO and glass pH electrode. The L_2-eRuO electrode showed reliable potentiometric pH response including near Nernstian behavior (slope=−60.5 mV pH^{-1}, r=0.9997) and reasonable response time ($t_{90\%}$=ca. 6.5±2.0 s). The pH response of L_2-eRuO on Au wire electrode (0.5 mm in diameter) also revealed a slope of −55.2 mV pH^{-1}, which showed the possibility of miniaturization for local pH sensing [24]. Note that the reported value for L_2-ePt showed a slope of −51 mV pH^{-1} and response time of $t_{95\%}$=ca. 60 s [20].

Conclusions

We have sucessfully synthesized L_2-eRuO directly grown on Au substrates using an electrochemical deposition of $RuCl_3$ in the presence of reverse micelles of Triton X-100. FE-SEM and HR-TEM images of L_2-eRuO show apparent

grain and pores (2.3±0.2 nm) contrast to that of L_2-ePt where no apparent grain or pore was observed. The facile and simple approach described in this study not only allows controllable variation of the *Rf* to achieve optimum performance, but also eliminates complicated experimental procedures and purification steps. The surface area of the electrodes was estimated by Cu UPD, showing high RSA which favors to obtain larger electrochemical response of glucose and better selectivity over AA, AP, UA and DA, due to the enlarged active surface area for the kinetically slow glucose oxidation. The optimized L_2-eRuO electrode (*Rf*=320) exhibited 17 fold higher total current responses for amperometric glucose detection compared to the RuO electrode, with a sensitivity of 40.2 $\mu A\ mM^{-1}\ cm^{-2}$ (normalized to GSA) in a linear range of zero to 4 mM glucose. Compared to the reported value for L_2-ePt, the prepared L_2-eRuO electrode also showed better potentiometric responses to pH changes, such as a steeper potential shift per pH, and a faster response time as well as facility of miniaturization for possible microsensor due to the increased surface area.

Acknowledgements This research was supported by Basic Reaserch Program through the National Reasearch Foundation of Korea (NRF) funded by the Ministry of Education, Science and Technology (2011–0009741). This work was also supported by Mid-career Researcher Program through the National Research Foundation of Korea (NRF) funded by the Ministry of Education, Science and Technology (2011–0015619).

References

1. Park S, Boo H, Chung TD (2006) Electrochemical non-enzymatic glucose sensors. Anal Chim Acta 556:46–57, and references therein
2. Walcarius A, Kuhn A (2008) Ordered porous thin films in electrochemical analysis. Trends Anal Chem 27:593–603
3. Park S, Chung TD, Kim HC (2003) Nonenzymatic glucose detection using mesoporous platinum. Anal Chem 75:3046–3049
4. Park S, Lee Y, Boo H, Kim HM, Kim KB, Kim HC, Song YJ, Chung TD (2007) Three-dimensional interstitial nanovoid of nanoparticulate Pt film electroplated from reverse micelle solution. Chem Mater 19:3373–3375
5. Park S, Song YJ, Han JH, Boo H, Chung TD (2010) Structural and electrochemical features of 3D nanoporous platinum electrodes. Electrochim Acta 55:2029–2035
6. Wang J, Thomas DF, Chen A (2008) Nonenzymatic electrochemical glucose sensor based on nanoporous PtPb networks. Anal Chem 80:997–1004
7. Xiao F, Zhao F, Mei D, Mo Z, Zeng B (2009) Nonenzymatic glucose sensor based on ultrasonic-electrodeposition of bimetallic PtM (M = Ru, Pd and Au) nanoparticles on carbon nanotubes-ionic liquid composite film. Biosens Bioelectron 24:3481–3486
8. Xm C, Zj L, Chen DJ, Tt J, Zm C, Xr W, Chen X, Gn C, Oyama M (2010) Nonenzymatic amperometric sensing of glucose by using palladium nanoparticles supported on functional carbon nanotubes. Biosens Bioelectron 25:1803–1808
9. Zhou YG, Yang S, Qian QY, Xia XH (2009) Gold nanoparticles integrated in a nanotube array for electrochemical detection of glucose. Electrochem Commun 11:216–219
10. Xia Y, Huang W, Zheng J, Niu Z, Li Z (2011) Nonenzymatic amperometric response of glucose on a nanoporous gold film electrode fabricated by a rapid and simple electrochemical method. Biosens Bioelectron 26:3555–3561
11. Shim JH, Cha A, Lee Y, Lee C (2011) Nonenzymatic amperometric glucose sensor based on nanoporous gold/ruthenium electrode. Electroanalysis 23:2057–2062
12. Lu LM, Li HB, Qu F, Zhang XB, Shen GL, Yu RQ (2011) In situ synthesis of palladium nanoparticle-graphene nanohybrids and their application in nonenzymatic glucose biosensors. Biosens Bioelectron 26:3500–3504
13. Su C, Zhang C, Lu G, Ma C (2010) Nonenzymatic electrochemical glucose sensor based on Pt nanoparticles/mesoporous carbon matrix. Electroanalysis 22:1901–1905
14. Bo X, Ndamanisha JC, Bai J, Guo L (2010) Nonenzymatic amperometric sensor of hydrogen peroxide and glucose based on Pt nanoparticles/ordered mesoporous carbon nanocomposites. Talanta 82:85–91
15. Qiu H, Xue L, Ji G, Zhou G, Huang X, Qu Y, Gao P (2009) Enzyme-modified nanoporous gold-based electrochemical biosensors. Biosens Bioelectron 24:3014–3018
16. Shim JH, Lee Y (2009) Amperometric nitric oxide microsensor based on nanopore-platinized platinum: the application for imaging NO concentrations. Anal Chem 81:8571–8576
17. Attard GS, Bartlett PN, Coleman NRB, Elliott JM, Owen JR, Wang JH (1997) Mesoporous platinum films from lyotropic liquid crystalline phases. Science 278:838–840
18. Elliott JM, Birkin PR, Bartlett PN, Attard GS (1999) Platinum microelectrodes with unique high surface areas. Langmuir 15:7411–7415
19. Choi KS, McFarland EW, Stucky GD (2003) Electrocatalytic properties of thin mesoporous platinum films synthesized utilizing potential-controlled surfactant assembly. Adv Mater 15:2018–2021
20. Han JH, Lee E, Park S, Chang R, Chung TD (2010) Effect of nanoporous structure on enhanced electrochemical reaction. J Phys Chem C 114:9546–9553
21. Trasatti S (2000) Electrocatalysis: understanding the success of DSA. Electrochim Acta 45:2377–2385
22. Dharuman V, Pillai KC (2006) RuO_2 electrode surface effects in electrocatalytic oxidation of glucose. J Solid State Electrochem 10:967–979
23. Mihell JA, Atkinson JK (1998) Planar thick-film pH electrodes based on ruthenium dioxide hydrate. Sens Actuators B 48:505–511
24. Lenz J, Trieu V, Hempelmann R, Kuhn A (2011) Ordered macroporous ruthenium oxide electrodes for potentiometric and amperometric sensing applications. Electroanalysis 23:1186–1192
25. Green CL, Kucernak A (2002) Determination of the platinum and ruthenium surface areas in platinum-ruthenium alloy electrocatalysts by underpotential deposition of copper. I. unsupported catalysts. J Phys Chem B 106:1036–1047
26. Zhang Y, Huang L, Arunagiri TN, Ojeda O, Flores S, Chyan O, Wallace RM (2004) Underpotential deposition of copper on electrochemically prepared conductive ruthenium oxide surface. Electrochem Solid-State Lett 7:C107–C110
27. Feast WJ (1986) The synthesis of conducting polymers. In: Skotheim TA (ed) Handbook of conducting polymers, vol 1. Marcel Dekker, New York
28. Han SJ, Jung HJ, Shim JH, Kim HC, Sung SJ, Yoo B, Lee DH, Lee C, Lee Y (2011) Non-platinum oxygen reduction electrocatalysts based on carbon-supported metal-polythiophene composites. J Electroanal Chem 655:39–44
29. Wooten M, Shim JH, Gorski W (2010) Amperometric determination of glucose at conventional vs. nanostructured gold electrodes in neutral solutions. Electroanalysis 22:1275–1277

30. Wang G, Wei Y, Zhang W, Zhang X, Fang B, Wang L (2010) Enzyme-free amperometric sensing of glucose using Cu-CuO nanowire composites. Microchim Acta 168:87–92
31. Chen X, Pan H, Liu H, Du M (2010) Nonenzymatic glucose sensor based on flower-shaped Au@Pd core-shell nanoparticles-ionic liquids composite film modified glassy carbon electrodes. Electrochim Acta 56:636–643
32. Babu TGS, Ramachandran T, Nair B (2010) Single step modification of copper electrode for the highly sensitive and selective nonenzymatic determination of glucose. Microchim Acta 169:49–55
33. Bai H, Han M, Du Y, Bao J, Dai Z (2010) Facile synthesis of porous tubular palladium nanostructures and their application in a nonenzymatic glucose sensor. Chem Commun 46:1739–1741
34. Li J, Yuan R, Chai Y, Che X, Li W, Zhong X (2011) Nonenzymatic glucose sensor based on a glassy carbon electrode modified with chains of platinum hollow nanoparticles and porous gold nanoparticles in a chitosan membrane. Microchim Acta 172:163–169
35. Sun J-Y, Huang K-J, Fan Y, Wu Z-W, Li D-D (2011) Glassy carbon electrode modified with a film composed of Ni(II), quercetin and graphene for enzyme-less sensing of glucose. Microchim Acta 174:289–294
36. Bo X, Bai J, Yang L, Guo L (2011) The nanocomposites of PtPd nanoparticles/onion-like mesoporous carbon vesicle for nonenzymatic amperometric sensing of glucose. Sens Actuators B 157:662–668